DOI 10.1007/s11204-024-09944-0
Soil Mechanics and Foundation Engineering, Vol. 61, No. 1, March, 2024 (Russian Original No. 1, January-February, 2024)

EVALUATING THE INTEGRITY OF SLAB–SOIL CONTACT WITH IMPULSE RESPONSE TESTING: INSIGHTS FROM NUMERICAL SIMULATIONS

UDC 620.179.17:624.073:550.344.33

A. A. Churkin,[1]* I. N. Lozovsky,[2] G. V. Volodin,[3] and R. A. Zhostkov[4]

[1]Gersevanov Research Institute of Bases and Underground Structures (NIIOSP), Research Centre of Construction JSC, Moscow, Russia; [2]Geoelectromagnetic Research Centre, Schmidt Institute of Physics of the Earth, Russian Academy of Sciences, Moscow, Russia; [3]Faculty of Geology, Lomonosov Moscow State University, Moscow, Russia; [4]Schmidt Institute of Physics of the Earth, Russian Academy of Sciences, Moscow, Russia,
*Corresponding author Email: chaa92@mail.ru.

To assess the sensitivity of impulse response testing to potential poor support zones or voids beneath the foundation slabs, numerical simulations were performed using the finite element method. These simulations covered a range of scenarios, including soil-loosening zones, sub-slab cavities, and slab cracks. The analysis of the simulation results employed two distinct techniques: the normalized acoustic response method and the ASTM C1740 mobility spectrum approach. These methods allowed the parameters and attributes derived from changes in input signals to be described in relation to the specifications within the synthetic models.

Introduction

Non-destructive methods of technical geophysics are utilized in the control of foundation slabs to assess the integrity of concrete and to identify zones where the structural contact with the underlying soil may be compromised [1–5]. One prevalent technique for addressing such concerns is the impulse response method, which involves recording and analyzing artificially induced transient vibrations of a concrete test element [2]. These vibrations are initiated through an impact source, most often a hammer, and are recorded by a transducer, typically a velocimeter or accelerometer.

The standardized method outlined in ASTM C1740 involves analyzing the mobility spectrum, which is determined by the ratio of the velocity spectrum (acquired from waveforms recorded by the transducer) to the force spectrum (obtained from waveforms recorded by the load cell attached to the hammerhead) [6–11]. In contrast, an alternative data collection and analysis approach [2–4] relies solely on examining the attributes of the velocity response normalized by the maximum value. This paper presents a study on the sensitivity of both approaches to poor support conditions, using synthetic data generated through finite-element numerical simulations.

Numerical Simulations

The numerical simulations of the spatial and temporal evolution of elastic wave fields are based on the predefined parameters of the "slab–soil" systems. Two-dimensional simulations were performed for a set of eight common contact disruption behaviors between foundation slabs and soil synthetic models (Fig. 1). The physical properties of the simulated materials were defined by the density (ρ) and the velocities of longitudinal and shear waves (V_p and V_s) [12–14], which were used to calculate the values of Young's modulus (E) and Poisson's ratio (ν) (Table 1).

The synthetic models consisted of the following key components [13, 15]:

– a foundation slab measuring 10 × 0.3 m (B30 concrete);

Translated from Osnovaniya, Fundamenty i Mekhanika Gruntov, No. 1, January-February, 2024.
0038-0741/24/6101-062

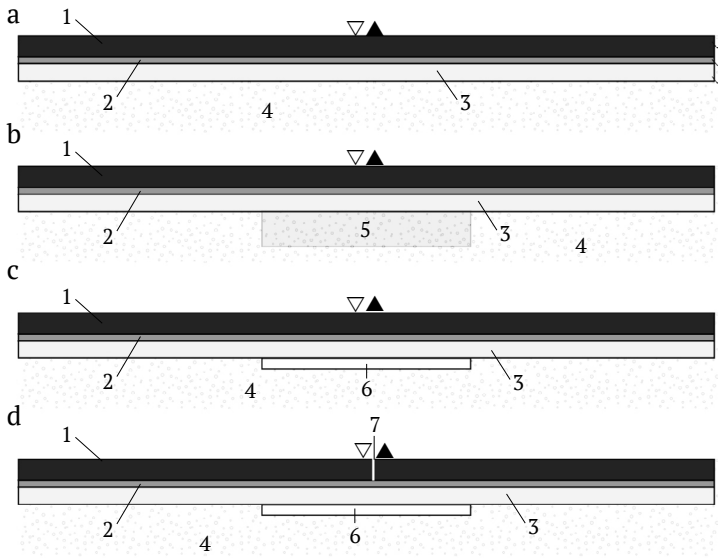

Fig. 1. Schematic representation of the "slab–soil" systems used for numerical simulations: a) model 0, b) models 1–5, c) model 6, d) model 7; ▽) source of elastic vibrations, ▲) transducer (velocimeter), 1) concrete slab (10 × 0.3 m; B30 concrete), 2) concrete sub-base (10 × 0.1 m; B7.5 concrete), 3) drainage layer (10 × 0.25 m; cement–sand mixture and gravel), 4) surrounding soil, 5) area of weakened soil (3 × 0.5 m), 6) void (3 × 0.15 m, air), 7) exit crack.

TABLE 1

Model No.	Material	V_p, m/s	V_s, m/s	h, m	ρ, kg/m^3	E, MPa	ν
0-7	B30 concrete (foundation slab)	3820	2630	0.3	2500	36000	0.17
	B7.5 concrete (sub-base)	2000	1330	0.1	2100	8199	0.17
	Cement–sand mixture and gravel (drainage layer)	1200	710	0.25	1300	1613	0.23
	Soil	750	440	0.5	1900	910	0.24
1	Weakened soil (disturbed area of uniformity)	640	350		1800	567	0.29
2		580	300		1700	403	0.32
3		550	270		1600	313	0.34
4		440	200		1500	164	0.37
5		370	160		1400	99	0.38
6	Air (void)	300	–	0.15	1.27	–	–
7	Through a crack in the slab, defined by a special solution in COMSOL Multiphysics						

– a concrete subbase measuring 10 × 0.1 m (B7.5 concrete);

– a drainage layer made of a cement–sand mixture and gravel, measuring 10 × 0.25 m;

– the surrounding soil.

Model 0 (reference model) represents a foundation slab supported by homogeneous soil. Models 1–5 introduce an area of weakened soil beneath the slab, measuring 3 × 0.5 m, with elastic properties decreasing as the model number increases [10, 14] (see Table 1).

Model 6 simulates a case of suffusion, where soil particles are washed away, creating a void (cavity) beneath the slab, measuring 3 × 0.15 m. Model 7 illustrates subsequent damage to the foundation slab.

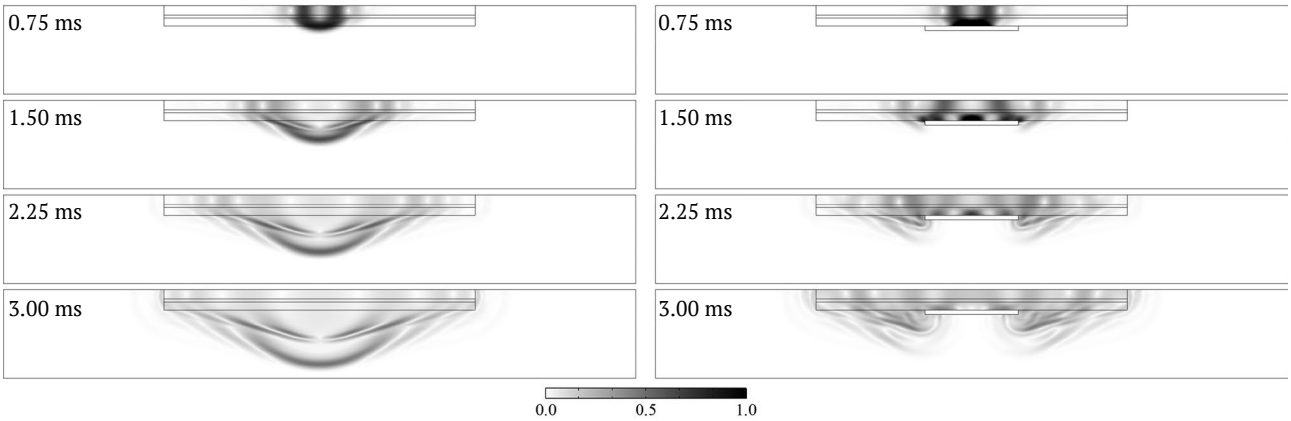

Fig. 2. Propagation of elastic waves in models 0 (left) and 6 (right) at 0.75, 1.50, 2.25, and 3.00 ms. The color scale represents the velocity values (in arbitrary units).

The numerical simulations were performed using the finite element method with COMSOL Multiphysics software. A unit vertical force, acting as an impulse source of elastic vibrations, was applied at the center of the slab. The vibration excitation utilized a Gaussian pulse modulated by a Hann window with a length of 0.8 ms [16]. Synthetic signal recordings were conducted with a virtual velocimeter placed 0.2 m to the right of the source. The recording duration was set to 7.5 ms. The upper boundary of the models was defined as stress free, except at the point of signal excitation. Conditions on the lower, left, and right boundaries were designed to be low-reflecting to minimize wave reflections from these regions.

The calculations were conducted on a structured grid. The size of the finite elements was determined to be 10% of the length of the shortest bulk wave possible in the considered medium, resulting in dimensions of 12.8×12.8 mm. Additional mesh refinement was applied in the boundary areas to provide detailed resolution of the transition processes, ensuring a predominant estimate of the numerical solution accuracy at 0.5%. The time step was set to 1.7 μs. Figure 2 illustrates the evolution of the elastic wave field excited in models 0 and 6.

Results

The results of numerical simulations of the vertical velocity component over time (signals recorded by the virtual velocimeter) are presented in Fig. 3. It is evident that the presence of weakened soil zones (models 1–5), a void beneath the slab (model 6), and an exit crack in the slab (model 7) significantly influence the responses captured during the simulations. In the time domain (Fig. 3a), additional features become apparent in the signals after 1 ms, with their intensity increasing with the model number. In the frequency domain (Fig. 3b), as the model number increases, there is a redistribution of amplitudes in the normalized spectra toward relatively high frequencies (around 1400 Hz), resulting in the emergence of prominent narrow peaks (models 6 and 7), as well as an increase in the intensity of the low-frequency component (within the frequency range 0–100 Hz).

The behavior of the attributes of velocity signals normalized by the maximum value, including the "voids index" parameter *vi* proposed in Churkin and Smirnov [3] and adapted from ASTM C1740 is as follows. The energy of the normalized signal, *En*, exhibits an increase of over 17% when transitioning from a homogeneous "slab–soil" contact (model 0) to the most significant soil loosening under the slab (model 5), and greatly increases with the presence of a void (models 6 and 7). Attribute *vi* follows a similar trend but demonstrates greater sensitivity, with a double increase from model 0 to model 5, in response to soil loosening underneath the slab. A normalized spectrum area attribute, denoted *Sn*, and the mean weighted frequency, referred to as *fs*, were computed for two distinct frequency ranges: 0–5000 and 0–800 Hz, as shown in Figs. 4b and 4c (solid and dashed lines respectively). The values of *Sn* decrease with an increase in the

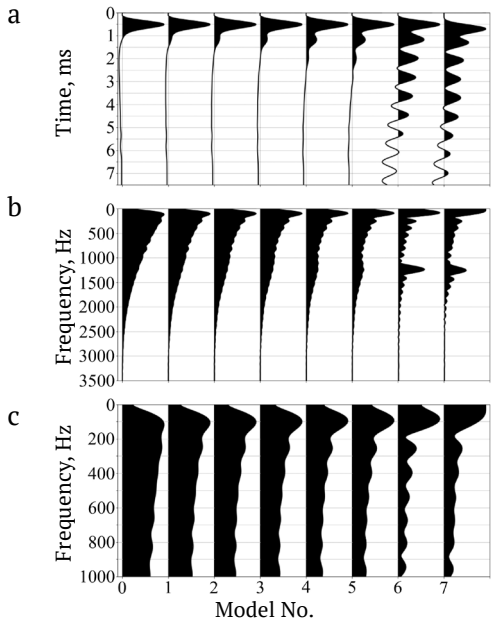

Fig. 3. Synthetic signals obtained from numerical simulations: a) signals in the time domain, normalized by their maximum values, b) amplitude spectra of the signals, normalized by their maximum values, c) mobility spectra.

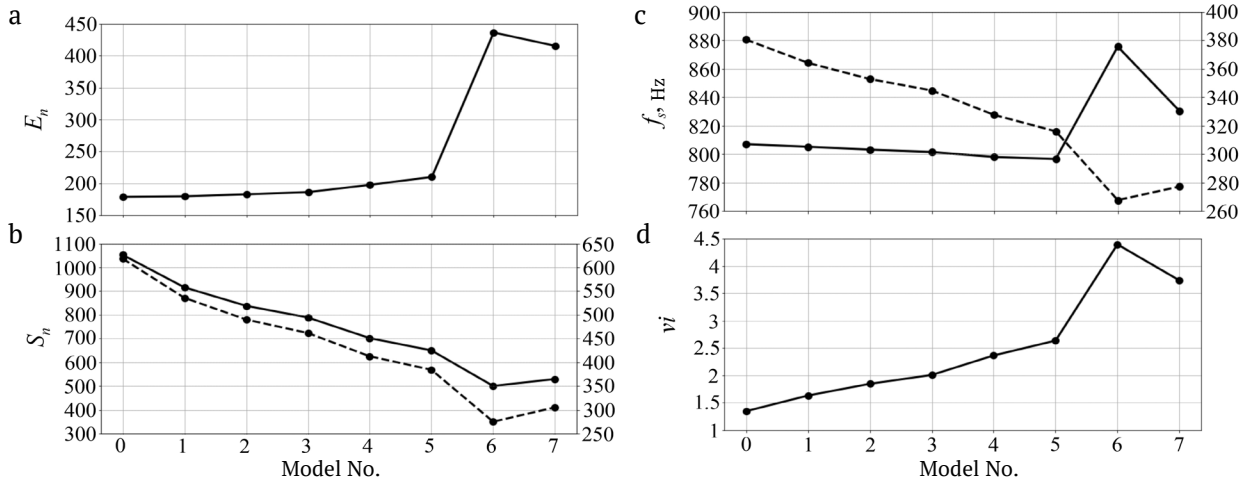

Fig. 4. Changes in normalized response attributes from model to model: a) energy of the normalized signal E_n, b) area of the normalized spectrum S_n, c) mean weighted frequency f_s, and d) voids index *vi*.

model number. Values of f_s, calculated for the 0–5000 Hz range, decrease slightly from model 0 to model 5 and increase for models with a void beneath the slab. When limiting the input frequency range to 0–800 Hz, f_s decreases with the model number, indicating changes in the low-frequency components of the signals.

The mobility spectra curves are shown in Fig. 3c. The shape of these curves undergoes significant alterations as the soil properties decrease, voids, and exit cracks appear. The intensity of the low-frequency component within the frequency range 0–100 Hz increases, whereas additional extremes become evident in the curves within the 200–800 Hz frequency range.

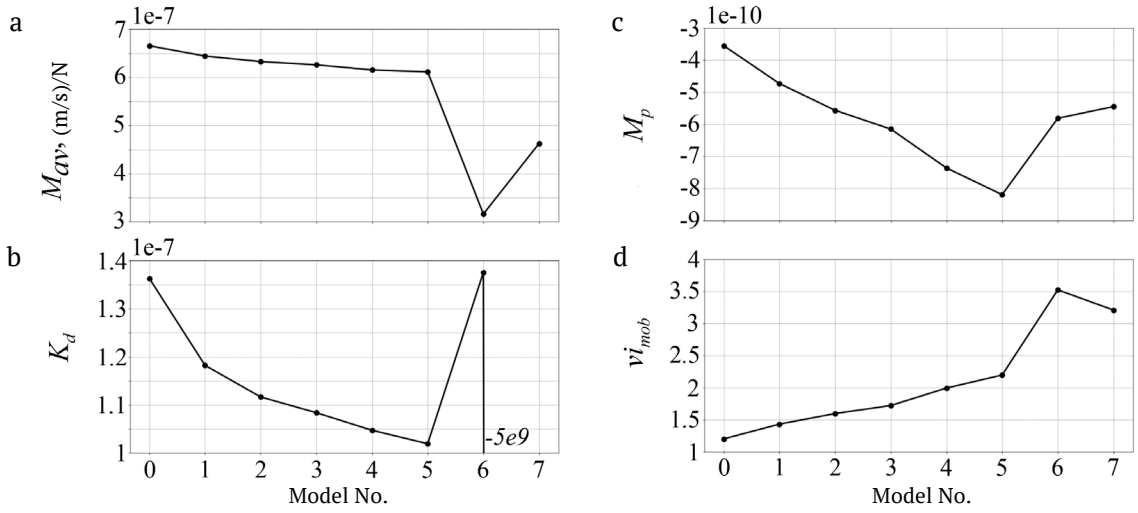

Fig. 5. Changes in mobility spectrum parameters from model to model: a) average mobility value of 100–800 Hz frequency range (M_{av}), b) dynamic stiffness (K_d), c) the slope within the frequency range 100–800 Hz (M_p), and d) voids index (vi_{mob}).

The mobility spectrum parameters (Fig. 5), calculated according to ASTM C1740 recommendations, included the average mobility value of 100–800 Hz frequency range M_{av}, curve inclination parameter K_d ("dynamic stiffness") of 0–40 Hz, the inclination of a best-fit line M_p ('mobility slope') calculated for the 100–800 Hz range, and the ratio of the peak mobility value vi_{mob} below 100 Hz and M_{av} ('voids index') [3, 6].

The variations in mobility curve parameters from one model to another allow for the identification of a void beneath the slab. This is indicated by a sharp decrease in M_{av} and an increase in vi_{mob} (the behavior of this parameter is effectively identical to the *vi* attribute, as seen in Figs. 4 and 5). Models 6 and 7 are characterized by anomalous K_d values and increased M_p compared with model 5. The weakening of the soil beneath the slab (models 1–5) leads to reduced K_d and M_p values while increasing vi_{mob}, with a minor impact on M_{av} values.

Conclusions

The outcomes of the numerical simulations have demonstrated that the analysis of attributes of the normalized velocity responses is effective for identifying voids and areas of loosened soil beneath the slab, with performance comparable with the widely employed mobility spectrum analysis technique standardized by ASTM C1740. Moreover, the graphs depicting the changes in attributes of the normalized velocity response from one model to another exhibit a simple pattern of either decreasing or increasing values. In contrast, the behavior of parameters of the mobility spectra, specifically K_d and M_p, undergoes a distinct change when examining models with voids beneath the slab. This may suggest the potential for more reliable defect localization using the normalized velocity response analysis. The inclusion of an exit crack in the model did not have a substantial impact on attribute values and did not complicate the localization of the void beneath the slab.

During the calculation of each of the numerical models, identical force impulses were used to generate elastic vibrations, which somewhat limits the comparison of the two distinct data analysis approaches presented in the paper. During field tests to minimize the impact of variations in hammer impacts on the values of attributes of the normalized velocity response, it is recommended to perform stacking of repeated records (repeatedly exciting vibrations with the transducer in a fixed position and subsequently averaging the attribute values obtained).

Future research avenues may involve the validation of numerical computations through physical experiments and the integration of three-dimensional numerical modeling techniques. These efforts are aimed at assessing the impact of edge effects and gaining a comprehensive understanding of the method's applicability when testing structures with diverse geometry and surrounding soil properties.

References

1. G. V. Volodin and V. V. Kapustin, "Oscillation analysis of foundation slabs to assess contact with soils," *Geotekhnika*, **13**, No. 4, 64-79 (2021), https://doi.org/10.25296/2221-5514-2021-13-4-64-79.
2. A. A. Churkin, A. Y. Khmel'nitskii, and V. V. Kapustin, "Evaluation of soil-structure contact state by normalized acoustic response analysis," *Soil Mech. Found. Eng.*, **59**, 453-458 (2022), DOI: 10.1007/s11204-022-09836-1.
3. A. Churkin and I. Smirnov, "Development of normalized acoustic response analysis for soil-structure contact state evaluation," *Earthq. Eng. Constr. Safety*, No 3, 32-47 (2023), DOI: 10.37153/2618-9283-2023-3-32-47.
4. I. N. Lozovsky and A. A. Churkin, "Multiscale entropy analysis for slab impulse response testing," *Bulletin of the Russian Academy of Sciences: Physics*, **87**, No. 10, 1518-1522 (2023), DOI: 10.3103/S1062873823703604.
5. A. A. Churkin, "Experience of low strain impact testing of piled raft foundation at the construction stage," *Soil Mech. Found. Eng.,* **60**, No. 4, 356-361 (2023).
6. ASTM C1740-16 Standard Practice for Evaluating the Condition of Concrete Plates Using the Impulse-Response Method (2016), DOI: 10.1520/C1740-16.
7. N. S. Ottosen, M. Ristinmaa, and A. G. Davis, "Theoretical interpretation of impulse response tests of embedded concrete structures," *J. Eng. Mech.*, No. 9, 1062-1071 (2004), DOI: 10.1061/(ASCE)0733-9399(2004)130:9(1062).
8. L. Sadowski, "Multi-scale evaluation of the interphase zone between the overlay and concrete substrate: methods and descriptors," *Appl. Sci.*, **9**, No. 7, 893 (2017), DOI: 10.3390/app7090893.
9. S. Sajid and L. Chouinard, "Impulse response test for condition assessment of concrete: A review," *Constr. Build. Mater.*, **211**, 317-328 (2019), DOI: 10.1016/j.conbuildmat.2019.03.174,
10. S. Sajid, A. Taras, and L. Chouinard, "Defect detection in concrete plates with impulse-response test and statistical pattern recognition," *Mechanical Systems and Signal Processing*, **161**, 107948 (2021), DOI: 10.1016/j.ymssp.2021.107948.
11. H. X. Tang, S. G. Long, and T. Li, "Quantitative evaluation of tunnel lining voids by acoustic spectrum analysis," *Constr. Build. Mater.*, **228**, 116762 (2019), DOI: 10.1016/j.conbuildmat.2019.116762.
12. J. H. Schon, *Physical Properties of Rocks*, Amsterdam, Elsevier (2011), DOI: 10.1016/S1567-8032(11)08006-2.
13. O. P. Afinogenov, A. O. Afinogenov, and A. A. Seryakova, "On the issue of determining the values of soils short-term elastic modulus for the calculation of road covers," *Molodoy Uchenyi,* **64**, No. 5, 41-43 (2014).
14. J. Bulinski and L. Sergiel, "Effect of moisture content on soil density — Compaction relation during soil compacting in the soil bin," *Ann. Wars. Univ. Life Sci.*, No. 64, 5-13 (2014).
15. S. Elkholy, B. El-Ariss, and S. Galal, "Structural performance of jointed reinforced concrete pavement slab with subbase erosion," *Structures*, No. 26, 982–995 (2020), DOI: 10.1016/j.istruc.2020.04.046.
16. E. Loseva, I. Lozovsky, R. Zhostkov, et al., "Wavelet analysis for evaluating the length of precast spliced piles using low strain integrity testing," *Appl. Sci.*, **12**, No. 21, 10901 (2022), DOI: 10.3390/app122110901.